

Neutrino signals from electroweak bremsstrahlung in solar WIMP annihilation

Nicole F. Bell,^a Amelia J. Brennan^a and Thomas D. Jacques^{a,b}

^aARC Centre of Excellence for Particle Physics at the Terascale
School of Physics, The University of Melbourne, Victoria 3010, Australia

^bDepartment of Physics and School of Earth and Space Exploration, Arizona State University, Tempe, AZ 85287-1404, USA

E-mail: n.bell@unimelb.edu.au, a.brennan@pgrad.unimelb.edu.au,
thomas.jacques@asu.edu

Abstract. Bremsstrahlung of W and Z gauge bosons, or photons, can be an important dark matter annihilation channel. In many popular models in which the annihilation to a pair of light fermions is helicity suppressed, these bremsstrahlung processes can lift the suppression and thus become the dominant annihilation channels. The resulting dark matter annihilation products contain a large, energetic, neutrino component. We consider solar WIMP annihilation in the case where electroweak bremsstrahlung dominates, and calculate the resulting neutrino spectra. The flux consists of primary neutrinos produced in processes such as $\chi\chi \rightarrow \bar{\nu}\nu Z$ and $\chi\chi \rightarrow \bar{\nu}\ell W$, and secondary neutrinos produced via the decays of gauge bosons and charged leptons. After dealing with the neutrino propagation and flavour evolution in the Sun, we consider the prospects for detection in neutrino experiments on Earth. By comparing our signal with that for annihilation to W^+W^- , we show that the detection prospects for the bremsstrahlung annihilation channel are favourable.

Contents

1	Introduction	1
2	Neutrino production	2
2.1	Dark matter coupling	3
2.2	Neutrino spectra at production	3
2.2.1	Primary neutrino spectra	4
2.2.2	Secondary neutrino spectra	4
3	Propagation in the Sun	6
3.1	Scattering and absorption	6
3.2	Flavour oscillations	7
4	Signals at Earth	9
4.1	Muon event rates	10
5	Conclusions	12

1 Introduction

High-energy neutrinos produced by dark matter (DM) self-annihilation in the Sun offer an appealing signal for indirect DM detection [1–8]. See, e.g., refs. [9–14] for recent work on this topic. DM particles which pass through the Sun can scatter, lose energy, and become captured by the gravitational field of the Sun. They accumulate in the Sun’s core and eventually reach a density where self-annihilation becomes important. Most Standard Model (SM) particles produced in the annihilations interact in the Sun and are hence absorbed, while neutrinos will escape to be detected in experiments on Earth. The neutrinos may be produced directly in the DM annihilations, or as secondaries in the decays of other SM particles. A high energy neutrino signal from the Sun would thus be a compelling indication of dark matter.

The strength of this signal is controlled by the DM-nucleon scattering cross section which controls the DM capture rate and, if in equilibrium, the annihilation rate. Existing limits have been placed by Super-Kamiokande [15], IceCube [16–18], and other experiments. The strength of these limits depend the annihilation channel assumed for dark matter, with limits for soft annihilation channels such as $\chi\chi \rightarrow \bar{b}b$ being weaker than those for hard channels such as $\chi\chi \rightarrow W^+W^-$. A comprehensive study of the neutrino spectra for the main annihilation channels with 2-body final states was performed in ref. [9]. In the present article we study DM annihilation processes with 3-body final states, namely bremsstrahlung processes in which a W or Z [19, 20] or γ [21–26] is radiated. In certain models, these bremsstrahlung processes have been shown to be the dominant DM annihilation mode.

For non-relativistic dark matter, it is useful to parametrise the thermally averaged annihilation cross section as

$$\langle v\sigma_A \rangle = a + bv^2 + \mathcal{O}(v^4), \quad (1.1)$$

where v is the dark matter velocity (in units of c). The a term arises only from s -wave annihilation, and the L^{th} partial wave contribution is suppressed by a factor v^{2L} . For highly non-relativistic DM with $v \ll 1$, s -wave annihilations, if permitted, are thus expected to

dominate. In the galactic halo, $v^2 \sim 10^{-6}$; v is even smaller for the DM accumulated in the solar core. However, in many Majorana DM models, s -wave annihilation to a pair of fermions, $\chi\chi \rightarrow ff$, is *helicity* suppressed by a factor of $(m_f/M_\chi)^2$ due to a mismatch between the net helicity and chirality of the fermion pair [27, 28]. A well known example is the annihilation of neutralino dark matter in supersymmetric models.

The circumstances in which annihilation to a pair of fermions is velocity and/or helicity suppressed were extensively detailed in ref. [20]. It is well known that radiation of a photon is able to lift this suppression via the electromagnetic (EM) bremsstrahlung process $\chi\chi \rightarrow \bar{f}f\gamma$ [21–26]. However, as shown in refs. [19, 20], electroweak (EW) bremsstrahlung is also able to lift this helicity suppression, such that the $\chi\chi \rightarrow \bar{f}fZ$, $\chi\chi \rightarrow f\nu W$, and $\chi\chi \rightarrow \bar{f}f\gamma$ annihilation channels all dominate over $\chi\chi \rightarrow \bar{f}f$. Physically, the suppression is lifted because the emitted gauge boson carries away a unit of angular momentum, allowing a fermion spin-flip, so there is no longer a mismatch between the chirality of the leptons and their allowed 2-particle spin state. Relative to the 2-body process, the rate for the 3-body final state suffers a suppression factor from the radiating particle given by $\alpha/4\pi \sim 10^{-3}$. However, this may be more than compensated for by the consequent *removal* of the $(m_f/M_\chi)^2$ suppression factor.

The importance of these radiative corrections to the dark matter annihilation process have been examined in a number of recent papers [29–39], with a focus on the indirect detection of dark matter due to annihilations in the Galactic halo. Interestingly, a possible hint of an EM bremsstrahlung signal was found in recent Fermi data [40]. In the present paper we consider the indirect detection of dark matter via annihilation in the Sun, noting that the EW bremsstrahlung annihilation channels produce large, energetic, neutrino fluxes.

This paper aims to produce the final neutrino energy spectra, as they would be detected on Earth, for solar WIMP annihilation via the EW bremsstrahlung process, and to compare the resulting signal with that for other commonly assumed annihilation channels. In section 2 we describe the neutrino spectra at production, including primary neutrinos produced directly in the annihilations, and secondaries produced from the decay of emitted gauge bosons. In section 3 we consider the scattering and flavour evolution of the neutrinos as they propagate through the Sun, and we present our main results in section 4, including a comparison of event rates with other DM annihilation models. These results are summarised briefly in section 5.

2 Neutrino production

During the process of capture in the Sun, DM particles scatter elastically with solar nuclei, losing enough energy to become gravitationally bound. The capture rate is proportional to the DM/solar nucleon scattering cross section and the local DM density, ρ_{DM}

$$\Gamma_{\text{cap}} \propto \sigma_{\text{scattering}} \rho_{\text{DM}}. \quad (2.1)$$

The DM becomes concentrated in a region of size $\sim 0.01 R_\odot \sqrt{100 \text{ GeV}/M_\chi}$, where R_\odot is the solar radius; the region is sufficiently small that we may assume all DM annihilations occur in the centre of the Sun [9].

The differential neutrino flux is given by

$$\frac{dN_\nu}{dE} = \frac{\Gamma_{\text{ann}}}{4\pi d^2} \sum_k \text{BR}_k \frac{dN_k}{dE}, \quad (2.2)$$

where d is the distance from the centre of the Sun to the detector, and BR_k is the branching ratio to a specific final state, k . The annihilation rate Γ_{ann} depends on the capture rate Γ_{cap} as

$$\Gamma_{\text{ann}} = \frac{\Gamma_{\text{cap}}}{2} \tanh^2(t_0/\tau_A), \quad (2.3)$$

where $t_0 = 4.5$ Gyr is the age of the Sun and τ_A is the time-scale for competing capture and annihilation processes (see [6, 9, 41–43] for explicit calculations). This time-scale is typically much smaller than t_0 , so an equilibrium is reached between the capture and annihilation processes with $\Gamma_{\text{cap}} \simeq \Gamma_{\text{ann}}/2$. Therefore, the intensity of the annihilation signal will act as a probe of the DM scattering cross section on nucleons [2, 6].

2.1 Dark matter coupling

We use the leptophilic Majorana DM coupling of ref. [44] as a simple example of a scenario in which EW bremsstrahlung dominates the annihilation. The DM is a gauge-singlet Majorana fermion which annihilates to leptons via the interaction term

$$f(\nu \ l^-)_L \varepsilon \begin{pmatrix} \eta^+ \\ \eta^0 \end{pmatrix} \chi + h.c. = f(\nu_L \eta^0 - l_L \eta^+) \chi + h.c. , \quad (2.4)$$

where f is a coupling constant, ε is the 2×2 SU(2) invariant antisymmetric matrix, and (η^+, η^0) form a new $SU(2)$ doublet scalar which mediates the annihilation. An identical coupling arises in supersymmetric models if we take χ to be a (bino-like) neutralino and η a sfermion doublet.

Ref. [44] proposed this model as an explanation of the sharp excess in the cosmic ray $e^+/(e^- + e^+)$ fraction at energies beyond ~ 10 GeV, as recently measured by the PAMELA experiment [45–47]. Here we adopt this model as a simple prototype of the situation in which bremsstrahlung processes dominate the DM annihilation. As explained in [19, 20], the s -wave contributions to the lowest order annihilation processes $\chi\chi \rightarrow \bar{\nu}\nu, e^+e^-$ are suppressed by factors of $(m_l/M_\chi)^2$. Bremsstrahlung lifts this suppression to become the dominant annihilation process.

We shall consider three possibilities for flavour structure of the branching ratios: DM annihilates to all three lepton flavours equally (branching fraction of $\frac{1}{3}$ to each), to electron-flavoured leptons only (branching fractions of 1, 0 and 0 to e, μ and τ flavours respectively), or to μ and τ flavours equally (branching fractions 0, $\frac{1}{2}, \frac{1}{2}$). However, we shall see that neutrino mixing reduces the sensitivity of the final results to the flavour structure of the couplings.

2.2 Neutrino spectra at production

We determine the energy spectra for the neutrinos at production by adding the contributions from the primary neutrinos produced directly in DM annihilation, and the secondary neutrino produced by decays of gauge bosons or charged leptons. Throughout, we neglect neutrinos with energies less than ~ 0.5 GeV. Note that IceCube, for example, has a detection threshold of ~ 100 GeV [48], which is reduced to ~ 10 GeV with the addition of DeepCore [49]. We shall be particularly interested in the higher-energy regions of the spectra, as the bremsstrahlung process leads to neutrino spectra with a distinct high energy peak; moreover, detection cross sections grow (approximately linearly) with energy.

2.2.1 Primary neutrino spectra

We first consider the primary neutrinos, those produced from the direct DM annihilation channels:

$$\begin{aligned}
\chi\chi &\rightarrow l^- \nu_l W^+ , \\
\chi\chi &\rightarrow l^+ \bar{\nu}_l W^- , \\
\chi\chi &\rightarrow \nu_l \bar{\nu}_l Z .
\end{aligned}
\tag{2.5}$$

The spectra of primary neutrinos from these processes are given in [19], along with calculations for the relative cross sections. The contribution from each bremsstrahlung channel is included according to these relative cross sections; for example the branching ratio for emission of a W^- is given by $\sigma_{e\nu W}/\sigma_{\text{total}}$, where σ_{total} is found by adding all the bremsstrahlung components together (including the contributions from $\chi\chi \rightarrow l^+ l^- Z$ and $\chi\chi \rightarrow l^+ l^- \gamma$, which do not produce primary neutrinos). Annihilation directly to neutrinos via the suppressed process $\chi\chi \rightarrow \nu\bar{\nu}$ would produce a monoenergetic spectrum with $E_\nu = M_\chi$; we neglect the contribution of this subdominant process in our analysis.

As an example, the primary spectra of muon neutrinos are indicated by the dashed green line in figure 1(a). The spectra have a broad energy distribution, and a distinctive high energy peak at $x \simeq 1$. Note that the primary neutrinos are the dominant contribution to the total neutrino spectrum for each flavour (shown as the solid blue line in figure 1(a)), particularly for the high-energy region of interest. In figure 1(a) we assume equal branching to all lepton flavours, and so the primary spectra are flavour-independent; changing the branching ratios will clearly affect the flavour dependence. Comparing the spectra for different choices of the DM mass, we see that the primary spectra maintain the same general shape. However, increasing the DM mass relative to $M_{W/Z}$ decreases the effect of kinematic thresholds and moves the peak closer to $x = 1$. The antineutrino spectra are identical to the corresponding neutrino spectra.

2.2.2 Secondary neutrino spectra

We next consider the secondary neutrinos that are produced from gauge boson decays, or the decays of primary tau leptons. The decay of the emitted gauge boson is modelled using the Monte Carlo simulator PYTHIA [50], in which we create a W or Z at rest which is then allowed to decay with constraints to be outlined below. The neutrino spectra from the gauge boson decays are then boosted into the lab frame as per the appendix of ref. [20]. In the Sun, the core density is $\rho = 140 \text{ g cm}^{-3}$, so energy loss processes are relatively important as the DM annihilation products may interact with solar material and lose energy before decaying further. Adopting a procedure similar to that in ref. [9], the relevant energy losses are accounted for as described below.

Gauge bosons: Once produced, the lifetimes of the W and Z bosons are short enough that they decay before interacting and losing any significant amount of energy. Therefore, in PYTHIA, we set these bosons to decay as if in vacuum. The products of the hadronic decay modes of the gauge bosons are dealt with as explained below.

Charged leptons: The typical stopping time of a charged lepton is $\tau_{\text{stop}} \sim 10^{-11} \text{ s}$. If this is shorter than the boosted lifetime, $\tau_{\text{stop}} < \gamma\tau_{\text{dec}}$, the lepton will lose all its energy before decaying. For the energy range of interest, $E \lesssim 1 \text{ TeV}$, the muons are stopped before they decay while taus decay without losing a significant amount of energy. Thus, in the PYTHIA routine, we discard electrons and muons, and allow taus to decay as if in vacuum.

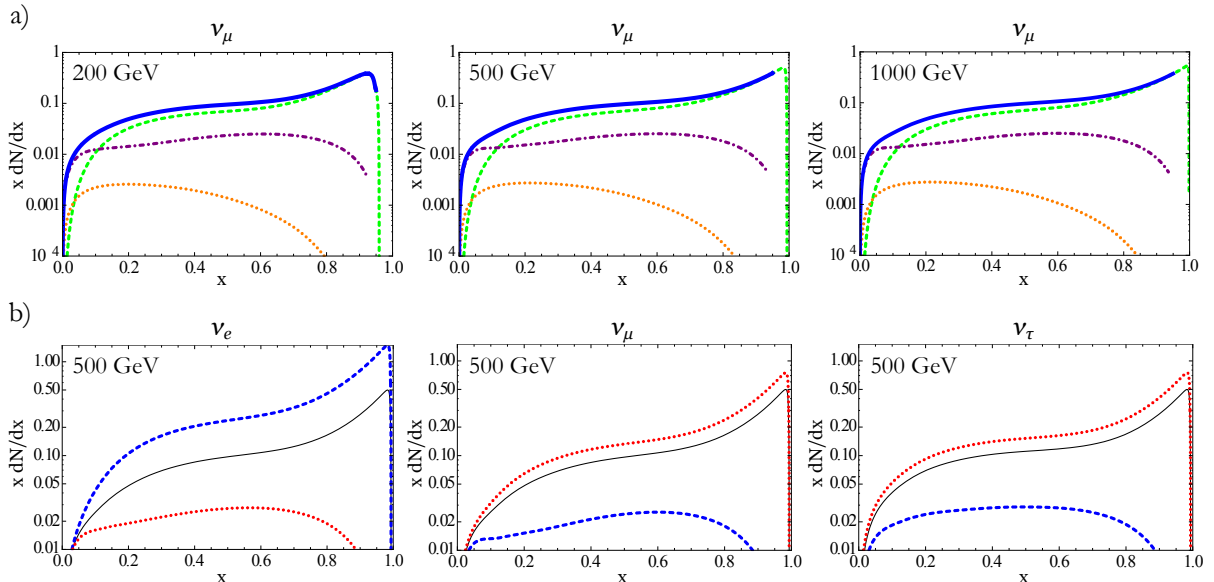


Figure 1. a) The contributions to the injected spectra, assuming branching to all lepton flavours equally, from primary neutrinos (green, dashed), secondary neutrinos from gauge boson decay (purple, dot-dashed) and secondary neutrinos from decay of primary taus (orange, dotted); the solid blue line shows the total. b) The total injected spectra for different branching ratios: annihilation to all lepton flavours equally (black, solid), annihilation to e -flavoured leptons only (blue, dashed), and annihilation to μ and τ flavours equally (red, dotted). All anti-neutrino spectra are identical to the corresponding neutrino spectra, and so are not shown. Note that the x -axis is defined as $x \equiv E_\nu/M_\chi$.

Quarks: Heavy hadrons have comparable τ_{stop} and $\gamma\tau_{\text{dec}}$, of order 10^{-11}s and 10^{-12}s respectively, so will often lose some energy before decaying; light hadrons are usually stopped before decay. As a reasonable, simple, approximation, we allow heavy hadrons (those including charm, top and bottom quarks) to decay, while light hadrons are discarded.

The resulting neutrino spectra from W^\pm and Z decay, as seen in the lab frame, are shown by the dot-dashed purple line in figure 1(a). These secondary neutrinos pile up and become dominant at low energies, as they are often produced through a chain of decays starting at the gauge boson. For this case of even branching ratios ($f_e = f_\mu = f_\tau$) the secondary spectra of ν_e and ν_μ are equal, as light hadrons and muons are stopped before decay, while τ , c and b produce equal numbers of each. As with the primary neutrinos, the antineutrino spectra are identical to their corresponding neutrino spectra.

In the case where the coupling f_τ is non-zero, there will be a primary tau component which will decay to contribute to the secondary neutrino flux. As with the gauge bosons decays, the secondary neutrino spectra from tau decay (again created using PYTHIA) must be boosted into the lab frame and convolved with the primary tau spectrum. The neutrino spectra resulting from this process are shown by the dotted orange line in figure 1(a). The tau decays make a minor contribution to the ν_e and ν_μ fluxes and a larger, though still subdominant, contribution to the ν_τ flux.

Adding the contributions of primary and secondary neutrino fluxes, we plot the total spectra at production as the solid blue line in figure 1(a). The total spectra are also shown in figure 1(b) for varied branching ratios: annihilation to all lepton flavours equally (black, solid), to e -flavoured leptons only (blue, dashed), and to μ and τ flavours equally (red, dotted). The primary neutrinos make the dominant contribution to the total flux. E.g., branching only to the electron flavour gives a large ν_e flux, with smaller ν_μ and ν_τ components

consisting only of secondary neutrinos.

3 Propagation in the Sun

Following production, the neutrino flux is modified by flavour oscillations, and by scattering with solar nuclei, which results in some absorption of the flux at high energy. These effects are well-understood, and various techniques exist to deal with them; we shall follow the method of ref. [51] to account for the scattering interaction, and then adopt results of ref. [52] when evaluating the flavour evolution. Many authors combine scattering and mixing effects into a single 3×3 density matrix equation that describes the neutrino evolution. However in the energy range of interest, $E_\nu \lesssim 1$ TeV, oscillations and scattering approximately decouple [51], as the matter effects in the Sun ensure negligible mixing between ν_e and $\nu_{\mu,\tau}$ until *after* scattering becomes unimportant. We assume throughout that the ν_μ and ν_τ fluxes are equal, as ν_μ and ν_τ mix maximally (to good approximation) and, for the energy range of interest, the oscillation length is less than or approximately equal to the interaction length [51].

3.1 Scattering and absorption

The evolution equation, used to evolve the neutrino flux from production to r_c (the radius where interactions become unimportant), has the form

$$\frac{\partial \rho_l}{\partial r} = \frac{\partial \rho_l}{\partial r} \Big|_{\text{inj}} + \frac{\partial \rho_l}{\partial r} \Big|_{\text{NC}} + \frac{\partial \rho_l}{\partial r} \Big|_{\text{CC}}, \quad (3.1)$$

for neutrinos of flavour l , where $\rho(r, E)dE$ is the neutrino flux. The first term on the right corresponds to the neutrino injection due to the annihilation of DM (including all secondary neutrinos). The second and third terms correspond to neutrino scattering through neutral current and charged current interactions respectively.

The probability of an interaction between a neutrino and a solar nucleon is given by

$$P_{\text{int}} = \int_0^{R_\odot} \sigma_{\text{tot}}(E) N_S(r') dr' = \frac{E}{\mathcal{E}}, \quad (3.2)$$

where σ_{tot} is the neutrino total interaction cross section and $N_S(r) \simeq N_0 e^{-r/\kappa R_\odot}$ is the nucleon density of the Sun, with $\kappa = 0.1$ and $N_0 = 1.3 \times 10^{26} \text{ cm}^{-3}$. The constants \mathcal{E} parametrise the energy scale at which interactions become significant, and are given by

$$\mathcal{E}_\nu \simeq 140 \text{ GeV}, \quad \mathcal{E}_{\bar{\nu}} \simeq 213 \text{ GeV}. \quad (3.3)$$

Note that the total interaction cross section combines neutral current (NC) scatterings $\nu_l N \leftrightarrow \nu_l N$ and $\bar{\nu}_l N \leftrightarrow \bar{\nu}_l N$ (effectively removing a neutrino from the flux and re-injecting it at lower energy), and charged current (CC) scatterings $\nu_l N \leftrightarrow l^- N'$ and $\bar{\nu}_l N \leftrightarrow l^+ N'$ (effectively removing a neutrino from the flux and producing an almost collinear charged lepton). If $l = e, \mu$ then the final lepton loses most, if not all, of its energy before it can decay again, and so the neutrino is considered absorbed. If $l = \tau$, the resulting τ^\pm decays promptly, either leptonically or hadronically.

Defining the optical depth as

$$y(r) \equiv \frac{1}{N_0 \kappa R_\odot} \int_0^r N_S(r') dr', \quad (3.4)$$

the evolution equation (3.1) takes the form

$$\frac{\partial \rho_j}{\partial y} = h(E) + \frac{1}{\mathcal{E}} \left[-E \rho_j(y, E) + \int_E^\infty dE' g_j(E/E') \rho_j(y, E') \right]. \quad (3.5)$$

The term $h(E)$ represents our injected flux, the second term accounts for absorption of the flux through scattering, and the last term the reinjection or regeneration of neutrinos at lower energy. At high energies, absorption through scattering is a significant effect. Tau regeneration is also important, as absorbed neutrinos are repopulated and pile-up at lower energies. Again, this effect is most significant for large DM mass. The regeneration functions g_i are given, e.g., in refs. [9, 51]. Following ref. [51] we use a perturbative solution of eq. (3.5) to handle the regeneration. For simplicity, we take $g_i = 0.5$ and have checked that for the largest M_χ we consider (where regeneration is expected to occur most strongly) this simplification produces an error $<20\%$ in the final spectra for energies $\gtrsim 100$ GeV, which does not qualitatively change our conclusions.

3.2 Flavour oscillations

We now include the effect of neutrino flavour mixing. We use the neutrino mixing parameters given in ref. [53], and assume the normal mass hierarchy, where $m_1 < m_2 < m_3$. We shall adopt a non-zero value for θ_{13} , as indicated by recent results from the T2K [54] and the Daya Bay [55] collaborations, and demonstrate how the results change as we vary the value of this parameter.

Neutrinos undergo flavour conversion during their propagation through the Sun. These flavour effects differ from oscillations in vacuum due to the presence of neutrino refractive indices. In the dense solar medium, the electron neutrinos experience a matter potential of $V_e(r) = \sqrt{2}G_F N_e(r)$, where N_e is the electron number density. At high density, this leads to an approximate alignment between the flavour and effective mass eigenstates, and suppresses oscillations of ν_e with $\nu_{\mu,\tau}$. The matter potential decreases as the neutrinos propagate outward from the centre of the Sun, and the neutrinos undergo an MSW resonance [56, 57] when

$$\Delta m^2/2E \simeq V_e. \quad (3.6)$$

At low energies, the propagation through this resonance is adiabatic and the neutrinos remain in given mass eigenstates. At higher energies the evolution becomes non-adiabatic, with the neutrinos experiencing a level-crossing, or jump between mass eigenstates. Assuming an exponentially varying solar profile ($\rho(r) \propto e^{-r/r_0}$), with $r_0 = R_\odot/10.54$, the crossing probability is conventionally given by [58]

$$P_C = \frac{e^{\gamma \cos^2 \theta} - 1}{e^\gamma - 1}, \quad \gamma = 4\pi r_0 \Delta, \quad (3.7)$$

where $\Delta \equiv \Delta m^2/4E\nu$. For antineutrinos, the $\bar{\nu}_e$ potential is $-V_e(r)$, which is equivalent to making the replacement $\theta \rightarrow \frac{\pi}{2} - \theta$ [59], thus

$$\bar{P}_C = P_C(\theta \rightarrow \frac{\pi}{2} - \theta). \quad (3.8)$$

We shall be concerned with two level crossings, controlled by Δm_{21}^2 and Δm_{32}^2 respectively. As Δm_{32}^2 is almost two orders of magnitude larger than Δm_{21}^2 the crossings decouple

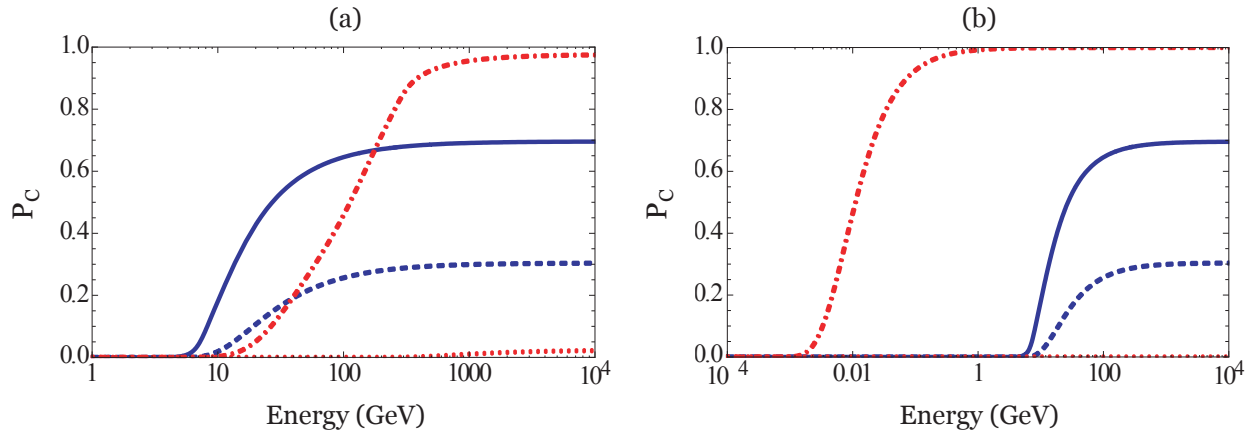


Figure 2. The level-crossing probabilities P_C ; our chosen value of $\theta_{13} = 8.8^\circ$ is used in fig (a), while fig (b) shows the corresponding result for $\theta_{13} = 0.1^\circ$. The first (θ_{13} -driven) level crossing probabilities (P_C^h) are shown by the red dot-dashed (neutrino) and dotted (antineutrino) lines, while the second (θ_{12} -driven) crossing probabilities (P_C^l) are shown by the blue bold (neutrino) and dashed (antineutrino) lines.

and can be treated independently. This separation is useful as it allows us to use a simple two-neutrino formalism which we apply to each crossing independently. This leads to

$$P = \begin{pmatrix} 1 - P_C^l & P_C^l & 0 \\ P_C^l & 1 - P_C^l & 0 \\ 0 & 0 & 1 \end{pmatrix} \begin{pmatrix} 1 & 0 & 0 \\ 0 & 1 - P_C^h & P_C^h \\ 0 & P_C^h & 1 - P_C^h \end{pmatrix}, \quad (3.9)$$

where P_{jk} represents the probability of a neutrino that originated in matter mass eigenstate k ending up in *vacuum* mass eigenstate j . Here, P_C^l and P_C^h correspond to the lower and higher level crossing probabilities, driven by θ_{12} and θ_{13} respectively. See ref. [60] for a detailed discussion.

We shall need to evaluate the level crossing probabilities for the two resonances, and for both neutrinos and antineutrinos. In some of these cases the resonance condition (3.6) is never actually met; nonetheless, the level crossing probability is non-zero and the expression given in eq.(3.7) still holds [52, 61, 62].¹ For some parameters of interest (namely, high neutrino energy) the lower level crossing takes place in the convective zone of the Sun where the solar density profile deviates from the exponential form assumed in eq. (3.7). We account for this by following the procedure developed in ref. [52], where P_C is calculated according to eq. (3.7), but with r_0 replaced by an energy-dependent numerical fit.

The level crossing probabilities, for neutrinos and antineutrinos, are plotted as a function of neutrino energy in figure 2. Figure 2(a) shows the probabilities used here, assuming $\theta_{13} = 8.8^\circ$, as suggested by recent T2K [54] and the Daya Bay [55] results, while figure 2(b) shows the probabilities if we instead allow $\theta_{13} = 0.1^\circ$. Note that for very small θ_{13} , P_C^h for neutrinos approaches 1 for all energies (i.e. the resonance is completely non-adiabatic). This is to be expected because as $\theta_{13} \rightarrow 0$ the heaviest vacuum eigenstate becomes completely decoupled, and does not mix with the other mass eigenstates. For antineutrinos $P_C^h \simeq 0$, as the resonance condition is never met. We also see that the lower crossing probabilities, P_C^l are comparatively larger for neutrinos than antineutrinos, as $\bar{\nu}_e$ is produced in the lightest matter mass eigenstate and, again, does not undergo a resonance.

¹As discussed in refs. [52, 62], the crossing probability is largest when adiabaticity is maximally violated, and is non-zero even away from resonance.

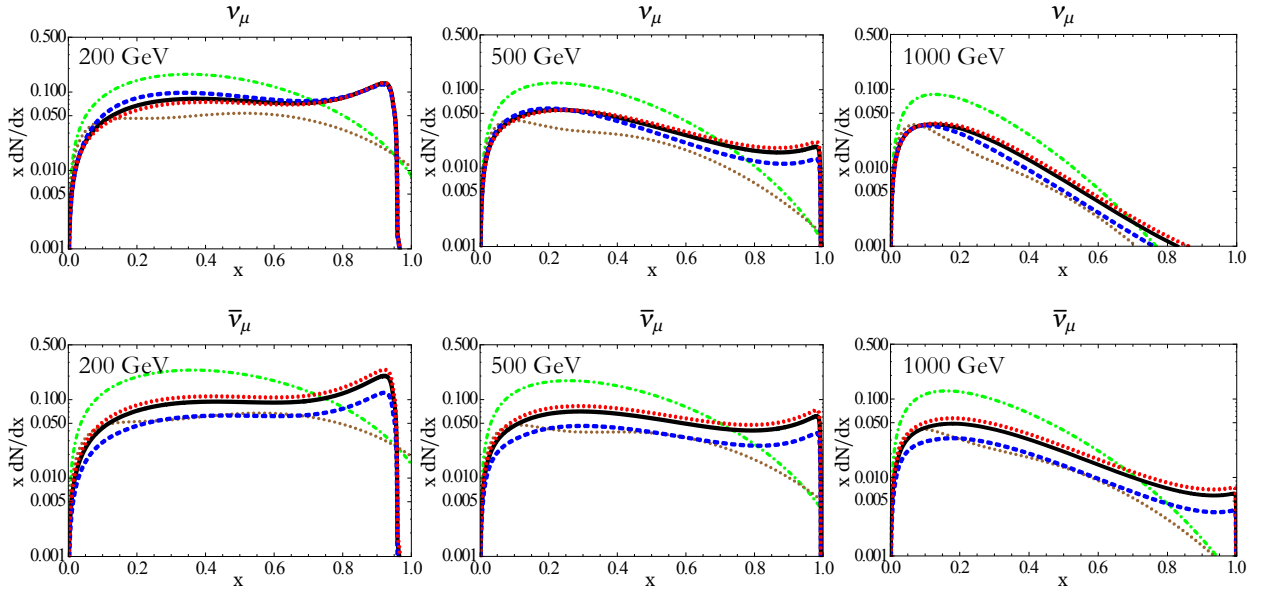


Figure 3. The final muon-flavour (anti)neutrino energy spectra, per annihilation, after propagation from the Sun’s centre to Earth, for $M_\chi = 200, 500, 1000$ GeV. The curves denote different annihilation branching ratios: equal branching to all lepton flavours (black, bold), branching only to electron flavour (blue, dashed), branching evenly to μ and τ flavours (red, bold dotted). Also shown for comparison are the spectra arising from DM annihilation directly to $\tau^+\tau^-$ (green, dot-dashed) and to W^+W^- (brown, dotted). We set $\theta_{13} \simeq 8.8^\circ$.

We apply eq. (3.9) to obtain the neutrino fluxes at the edge of the Sun, in the vacuum mass basis. The neutrinos propagate from the Sun to the Earth in these vacuum states, and can then be converted back to the flavour basis. The final spectra are shown in figure 3.

4 Signals at Earth

The final neutrino spectra for the electroweak bremsstrahlung annihilation mode are shown in figure 3, for various choices of the branching ratios to the lepton flavours. Also shown, for comparison, are the spectra from annihilation of DM to W^+W^- and $\tau^+\tau^-$ final states. These comparison spectra were calculated using the same procedure described in the previous section. The spectra shown are normalised per annihilation; the absolute normalisation is set by the DM capture rate Γ_{cap} (assuming equilibrium).

We note that while the initial spectra at production were sensitive to flavour branching ratios chosen, neutrino flavour mixing in the Sun considerably reduces these differences. For example, for branching only to the electron flavour, the only ν_μ and ν_τ components at production are secondary neutrinos. However, the flavour mixing that takes place via the level crossings serves to even out the distribution across the three flavours. The final spectra have a similar shape, irrespective of the branching ratios chosen, with magnitudes that vary by only a factor of $\lesssim 2$.

Scattering and absorption have a strong effect on the spectra for $M_\chi = 1000$ GeV, but very little effect for $M_\chi = 200$ GeV. This is expected as absorption depends exponentially on the neutrino energy. For large M_χ , the high energy regions of the spectra are strongly damped, removing the high energy peak. This is a bigger effect for neutrinos than for

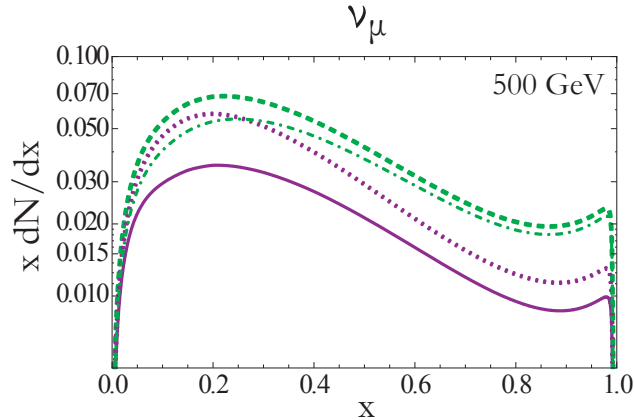


Figure 4. The ν_μ spectra for $M_\chi = 500$ GeV, for different choices of θ_{13} . For branching only to e -flavoured leptons the spectra are shown for $\theta_{13} = 0.1^\circ$ (purple, solid) and $\theta_{13} = 8.8^\circ$ (purple, dotted). For branching to μ and τ flavours equally the curves correspond to $\theta_{13} = 0.1^\circ$ (green, dashed) and $\theta_{13} = 8.8^\circ$ (green, dot-dashed). Note that there is no significant dependence on θ_{13} for the case of equal branching to all flavours.

antineutrinos due to the different values of \mathcal{E} — the scattering in the Sun affects neutrinos more strongly than their antiparticles. Overall, absorption significantly reduces the number of detectable neutrinos produced per annihilation. For the energies we consider, regeneration, which reintroduces neutrinos creating a pile-up at lower energies, is a smaller effect.

We now compare our spectra to those from other possible annihilation channels, $\chi\chi \rightarrow W^+W^-$ and $\chi\chi \rightarrow \tau^+\tau^-$. These channels have been chosen for comparison as they both have relatively hard neutrino spectra, with a significant flux at large values of x . As a result the existing limits on these channels are more stringent than those with softer neutrino spectra. The EW bremsstrahlung, W^+W^- and $\tau^+\tau^-$ channels all have broad energy spectra, of similar shape and scale. However EW bremsstrahlung channel has a significant high energy peak at $x \sim 1$, which will improve its detectability compared to the W^+W^- mode for which limits are usually determined [15–17]. We estimate relative event rates in the following subsection.

These plots in figure 3 were produced assuming a value for θ_{13} of 8.8° . For the purposes of comparison, we also computed spectra for $\theta_{13} = 0.1^\circ$. In the $\theta_{13} \simeq 0$ limit, the evolution through the high energy θ_{13} -driven resonance is completely non-adiabatic, with $P_C^h \simeq 1$ for all energies of interest, while for the larger mixing angle the resonance is (partially) adiabatic for energies $\lesssim 1000$ GeV. In figure 4, we compare the neutrino spectra for the two choices of θ_{13} . Decreasing θ_{13} decreases the adiabaticity of the resonance, and increases the differences between the spectra for each flavour. This effect is most significant at low energies, where the level-crossing probabilities are small (see figure 2), while at high energies $P_C^h \rightarrow 1$ irrespective of the value of θ_{13} . For antineutrinos, there is very little sensitivity to θ_{13} as the θ_{13} -resonance condition is never met.

4.1 Muon event rates

We now consider muon event rates in a detector such as IceCube. While IceCube is able to detect neutrinos of all flavours via cascade events, we consider here only the muon-track events as they have the greatest detection probability, since the long muon range in ice allows the detection of muons created well outside the detector. We shall find it useful to compare

the *ratio* of event rates for the EW bremsstrahlung annihilation channel relative to those for the comparison W^+W^- and $\tau^+\tau^-$ modes. We note that our spectra have been computed per annihilation, and the final event rates will depend on the absolute normalisation of the spectra and hence on the (here unspecified) DM/solar nucleon scattering cross section. However, by comparing the ratio of events for various annihilation channels we can determine whether the detection prospects for the EW bremsstrahlung annihilation channel are enhanced relative to the other commonly discussed channels.

We estimate event rates following a similar procedure to that in refs. [51, 63–65]. A muon neutrino can undergo charged current scattering with a nucleon within the ice of the detector, to produce a muon with energy $E_\mu = E_\nu(1 - y)$, where y is the charged current inelasticity parameter. This muon will then propagate through the ice and lose energy, with a range given by

$$R_\mu(E_\mu, E_\mu^{\text{thr}}) = \frac{1}{\beta} \ln \left[\frac{\alpha + \beta E_\mu}{\alpha + \beta E_\mu^{\text{thr}}} \right], \quad (4.1)$$

where $\alpha = 2.0 \text{ MeV cm}^2/\text{g}$, $\beta = 4.2 \times 10^{-6} \text{ cm}^2/\text{g}$, and E_μ^{thr} is the muon energy detection threshold, taken to be 100 GeV. Therefore, the probability that a neutrino with energy E_ν creates a muon that is detected with an energy above E_μ^{thr} is given by

$$P(E_\nu, E_\mu^{\text{thr}}) = \rho_N N_A \sigma_{\text{nucleon}}(E_\nu) R_\mu(E_\nu(1 - y), E_\mu^{\text{thr}}), \quad (4.2)$$

where ρ_N is the target nucleon density, N_A is Avogadro's number, and $\sigma_{\text{nucleon}}(E_\nu)$ is the charged current scattering cross section in ice. Finally, the muon track event rate is proportional to

$$\int \frac{dN(E_\nu)}{dE_\nu} P(E_\nu, E_\mu^{\text{thr}}) A^{\text{eff}} dE_\nu \quad (4.3)$$

where A^{eff} is the effective area of the detector; for IceCube this is $\sim 1 \text{ km}^2$ [66]. The scattering cross section $\sigma_{\text{nucleon}}(E_\nu)$ is proportional to E_ν and, in ice, the neutrino cross section is approximately twice as large as that for antineutrinos. We choose the average values of y as tabulated in ref. [63], which are approximately ~ 0.45 and ~ 0.35 for neutrinos and antineutrinos respectively. As a result, the lower bound on the (anti)neutrino energies that will produce observable muons is

$$\begin{aligned} E_{\nu_\mu} &\geq E_\mu^{\text{thr}}/(1 - y_\nu), & E_{\bar{\nu}_\mu} &\geq E_\mu^{\text{thr}}/(1 - y_{\bar{\nu}}), \\ &\simeq 182 \text{ GeV}, & &\simeq 154 \text{ GeV}. \end{aligned} \quad (4.4)$$

The number of muon track events for the EW bremsstrahlung annihilation channel, normalised to the number of events from annihilation to W^+W^- or $\tau^+\tau^-$, are shown in table 4.1. Equal branching to all three flavours has been assumed, which renders the results insensitive to the value of θ_{13} . We see that the EW bremsstrahlung channel would produce more events than the W^+W^- channel, for all masses considered, with a ratio of ~ 4 at $M_\chi = 200 \text{ GeV}$. The enhancement is strongest for low dark matter masses, because only the high energy regions of the spectra are above the detection threshold, and hence the high energy peak in the EW bremsstrahlung spectrum dominates. The ratio is smaller for large M_χ , as the detection threshold then corresponds to smaller values of x , and absorption effects damp the spectra at high energy. ² Detection prospects for annihilation channels

²While $\tau^+\tau^-$ annihilation mode results in more events than W^+W^- (which is to be expected as τ decays produce more neutrinos than W decays) we note, however, that annihilation to $\tau^+\tau^-$ may be a helicity-suppressed process, and thus subdominant, in some models.

	200 GeV	500 GeV	1000 GeV
normalised to $\tau^+\tau^-$	1.8	1.2	0.6
normalised to W^+W^-	3.8	2.4	1.9

Table 1. The ratio of μ^\pm muon-track events for the EW bremsstrahlung annihilation channel in an IceCube-like detector, normalised to event rates for annihilation directly to $\tau^+\tau^-$ or to W^+W^- . For the EW bremsstrahlung annihilation channel, equal branching ratios to all lepton flavours was assumed.

which produce hard spectra, such as W^+W^- , are better than those for annihilation channels which produce much softer neutrino spectra, such as $\bar{q}q$. Given that the EW bremsstrahlung mode would result in more events than for W^+W^- , its detection prospects are promising.

5 Conclusions

High-energy neutrinos produced by the annihilation of dark matter captured in the Sun offer a useful dark matter search strategy. By comparing the predicted neutrino fluxes with future detections, we can potentially distinguish between different DM annihilation channels, thus providing information to discriminate among competing DM models.

DM annihilation is usually assumed to be dominated by annihilation to 2-body final states. However, there are important DM annihilation processes with 3-body final states, namely bremsstrahlung processes in which a W , Z or γ is radiated. The electroweak bremsstrahlung processes $\chi\chi \rightarrow \bar{f}fZ$ and $\chi\chi \rightarrow f\nu W$ have been shown to be the dominant DM annihilation mode in certain popular models in which the lowest order annihilation processes are helicity suppressed. In the context of solar WIMP annihilation, these electroweak bremsstrahlung annihilation channels produces large, energetic, fluxes of neutrinos.

We have computed the neutrino energy spectra resulting from DM annihilation via the electroweak bremsstrahlung channel. This consists of primary neutrinos produced directly in the annihilations, which have a distinguishing peak near the endpoint $E_\nu = M_\chi$, and secondary neutrinos produced in decays of annihilation products. By comparing the event rates for the electroweak bremsstrahlung annihilation channel with those for annihilation to W^+W^- , we have shown that the EW bremsstrahlung channel has the larger event rate per annihilation, and hence promising detection prospects.

Acknowledgments

AJB was supported by the Commonwealth of Australia and NFB by the Australian Research Council. We thank Thomas Weiler, Kalliopi Petraki, James Dent, Lawrence Krauss, Nicholas Setzer and Martin White for helpful discussions.

References

- [1] J. Silk, K. Olive, and M. Srednicki, *The photino, the sun, and high-energy neutrinos*, *Phys.Rev.Lett.* **55** (1985) 257–259.
- [2] W. H. Press and D. N. Spergel, *Capture by the Sun of a Galactic Population of Weakly Interacting Massive Particles*, *Astrophys.J.* **296** (1985) 679–684.

- [3] K. Freese, *Can scalar neutrinos or massive Dirac neutrinos be the missing mass?*, *Phys.Lett.* **B167** (1986) 295–300.
- [4] L. Krauss, M. Srednicki, and F. Wilczek, *Solar system constraints and signatures for dark-matter candidates*, *Phys.Rev.* **D33** (1986) 2079.
- [5] T. Gaisser, G. Steigman, and S. Tilav, *Limits on cold-dark-matter candidates from deep underground detectors*, *Phys.Rev.* **D34** (1986) 2206.
- [6] A. Gould, *Resonant Enhancements in WIMP Capture by the Earth*, *Astrophys.J.* **321** (1987) 571.
- [7] M. Srednicki, K. Olive, and J. Silk, *High-energy neutrinos from the sun and cold dark matter*, *Nucl.Phys.* **B279** (1987) 804–823.
- [8] M. Kamionkowski, *Energetic neutrinos from heavy-neutralino annihilation in the sun*, *Phys.Rev.* **D44** (1991) 3021–3042.
- [9] M. Cirelli, N. Fornengo, T. Montaruli, I. A. Sokalski, A. Strumia, et al., *Spectra of Neutrinos from Dark Matter Annihilations*, *Nucl.Phys.* **B727** (2005) 99–138, [[hep-ph/0506298](#)].
- [10] M. Blennow, J. Edsjö, and T. Ohlsson, *Neutrinos from WIMP annihilations obtained using a full three-flavor Monte Carlo approach*, *JCAP* **01** (2008) 021, [[arXiv:0709.3898](#)].
- [11] V. Barger, F. Halzen, D. Hooper, and C. Kao, *Indirect search for neutralino dark matter with high energy neutrinos*, *Phys.Rev.* **D65** (2002) 075022, [[hep-ph/0105182v1](#)].
- [12] R. Lehnert and T. J. Weiler, *Flavor Sensitivity to θ_{13} and the Mass Hierarchy for neutrinos from Solar WIMP Annihilation*, [[arXiv:1002.2441](#)].
- [13] A. Erkoca, M. Reno, and I. Sarcevic, *Muon fluxes from dark matter annihilation*, *Phys.Rev.* **D80** (2009) 043514, [[arXiv:0906.4364](#)].
- [14] V. Barger, J. Kumar, D. Marfatia, and E. M. Sessolo, *Fermion WIMPless Dark Matter at DeepCore and IceCube*, *Phys.Rev.* **D81** (2010) 115010, [[arXiv:1004.4573](#)].
- [15] **Super-Kamiokande** Collaboration, K. Abe et al., *An Indirect Search for WIMPs in the Sun using 3109.6 days of upward-going muons in Super-Kamiokande*, [[astro-ph/1108.3384](#)].
- [16] **IceCube** Collaboration, R. Abbasi et al., *Limits on a muon flux from Kaluza-Klein dark matter annihilations in the Sun from the IceCube 22-string detector*, *Phys.Rev.* **D81** (2010) 057101, [[astro-ph/0910.4480v1](#)].
- [17] **IceCube** Collaboration, R. Abbasi et al., *Limits on a muon flux from neutralino annihilations in the Sun with the IceCube 22-string detector*, *Phys.Rev.Lett.* **102** (2009) 201302, [[astro-ph/0902.2460v3](#)].
- [18] **IceCube** Collaboration, T. DeYoung, *Particle physics in ice with IceCube DeepCore*, *Nucl.Instrum.Meth. A* (2011) [[arXiv:1112.1053](#)].
- [19] N. Bell, J. Dent, A. Galea, T. Jacques, L. Krauss, and T. Weiler, *W/Z Bremsstrahlung as the Dominant Annihilation Channel for Dark Matter, Revisited*, *Phys.Lett.* **B706** (2011) [[arXiv:1104.3823](#)].
- [20] N. F. Bell, J. B. Dent, T. D. Jacques, and T. J. Weiler, *W/Z Bremsstrahlung as the Dominant Annihilation Channel for Dark Matter*, *Phys.Rev.* **D83** (2011) 013001, [[arXiv:1009.2584](#)].
- [21] L. Bergström, *Radiative Processes in Dark Matter Photino Annihilation*, *Phys.Lett.* **B225** (1989) 372.
- [22] R. Flores, K. Olive, and S. Rudaz, *Radiative processes in LSP annihilation*, *Phys.Lett.* **B232** (1989) 377–382.
- [23] E. Baltz and L. Bergström, *Detection of Leptonic Dark Matter*, *Phys.Rev.* **D67** (2003) 043516, [[hep-ph/0211325](#)].

- [24] T. Bringmann, L. Bergström, and J. Edsjö, *New Gamma-Ray Contributions to Supersymmetric Dark Matter Annihilation*, *JHEP* **0801** (2008) 049, [[hep-ph/0710.3169v3](#)].
- [25] L. Bergström, T. Bringmann, and J. Edsjö, *New Positron Spectral Features from Supersymmetric Dark Matter: A Way to Explain the PAMELA Data?*, *Phys.Rev.* **D78** (2008) 103520, [[astro-ph/0808.3725v3](#)].
- [26] V. Barger, Y. Gao, W. Keung, and D. Marfatia, *Generic dark matter signature for gamma-ray telescopes*, *Phys. Rev. D* **80** (Sep, 2009) 063537, [[hep-ph/0906.3009v2](#)].
- [27] H. Goldberg, *Constraint on the photino mass from cosmology*, *Phys.Rev.Lett.* **50** (1983) 1419–1422.
- [28] L. Krauss, *New constraints on “INO” masses from cosmology*, *Nucl.Phys.* **B227** (1983) 556–569.
- [29] N. F. Bell, J. B. Dent, T. D. Jacques, and T. J. Weiler, *Dark Matter Annihilation Signatures from Electroweak Bremsstrahlung*, *Phys.Rev.* **D84** (2011) 103517, [[arXiv:1101.3357](#)].
- [30] N. F. Bell, J. B. Dent, T. D. Jacques, and T. J. Weiler, *Electroweak Bremsstrahlung in Dark Matter Annihilation*, *Phys.Rev.* **D78** (2008) 083540, [[arXiv:0805.3423](#)].
- [31] V. Barger, W. Keung, and D. Marfatia, *Bremsstrahlung in dark matter annihilation*, *Phys.Lett.* **B707** (2012) [[arXiv:1111.4523](#)].
- [32] P. Ciafaloni and D. Comelli, *Sudakov Effects in Electroweak Corrections*, *Phys.Lett.* **B446** (1999) 278–284, [[hep-ph/9809321](#)].
- [33] P. Ciafaloni and A. Urbano, *TeV scale Dark Matter and Electroweak Radiative Corrections*, *Phys.Rev.* **D82** (2010) 043512, [[arXiv:1001.3950](#)].
- [34] P. Ciafaloni, D. Comelli, A. Riotto, F. Sala, A. Strumia, and A. Urbano, *Weak corrections are relevant for dark matter indirect detection*, *JCAP* **03** (2011) 019, [[arXiv:1009.0224](#)].
- [35] P. Ciafaloni, M. Cirelli, D. Comelli, A. De Simone, A. Riotto, and A. Urbano, *On the importance of electroweak corrections for Majorana dark matter indirect detection*, *JCAP* **06** (2011) 018, [[arXiv:1104.2996](#)].
- [36] P. Ciafaloni, M. Cirelli, D. Comelli, A. De Simone, A. Riotto, and A. Urbano, *Initial state radiation in Majorana Dark Matter annihilations*, *JCAP* (2011) 034, [[arXiv:1107.4453](#)].
- [37] M. Garny, A. Ibarra, and S. Vogl, *Antiproton constraints on dark matter annihilations from internal electroweak bremsstrahlung*, *JCAP* **07** (2011) 028, [[arXiv:1105.5367](#)].
- [38] M. Garny, A. Ibarra, and S. Vogl, *Dark matter annihilations into two light fermions and one gauge boson: general analysis and antiproton constraints*, [arXiv:1112.5155](#).
- [39] P. Ciafaloni, D. Comelli, A. De Simone, A. Riotto, and A. Urbano, *Electroweak bremsstrahlung for wino-like Dark Matter annihilations*, [arXiv:1202.0692](#).
- [40] T. Bringmann, X. Huang, A. Ibarra, S. Vogl, and C. Weniger, *Fermi LAT Search for Internal Bremsstrahlung Signatures from Dark Matter Annihilation*, [arXiv:1203.1312](#).
- [41] K. Griest and D. Seckel, *Cosmic Asymmetry, Neutrinos and the Sun*, *Nucl.Phys.* **B283** (1987) 681.
- [42] A. Bottino, G. Fiorentini, N. Fornengo, B. Ricci, S. Scopel, and F. Villante, *Does solar physics provide constraints to weakly interacting massive particles?*, *Phys.Rev.* **D66** (2002) 053005, [[hep-ph/0206211](#)].
- [43] J. Lundberg and J. Edsjö, *Weakly interacting massive particle diffusion in the solar system including solar depletion and its effect on Earth capture rates*, *Phys.Rev.* **D69** (2004) 123505, [[astro-ph/0401113](#)].
- [44] Q.-H. Cao, E. Ma, and G. Shaughnessy, *Dark Matter: The Leptonic Connection*, *Phys.Lett.*

- B673** (2009) 152–155, [[arXiv:0901.1334](#)].
- [45] **PAMELA** Collaboration, O. Adriani et al., *An Anomalous Positron Abundance in Cosmic Rays with Energies 1.5–100 GeV*, *Nature* **458** (2009) 607–609, [[arXiv:0810.4995](#)].
- [46] **PAMELA** Collaboration, O. Adriani et al., *PAMELA Results on the Cosmic-Ray Antiproton Flux from 60 MeV to 180 GeV in Kinetic Energy*, *Phys.Rev.Lett.* **105** (2010) 121101, [[arXiv:1007.0821](#)].
- [47] **PAMELA** Collaboration, O. Adriani et al., *A New Measurement of the Antiproton-to-Proton Flux Ratio up to 100 GeV in the Cosmic Radiation*, *Phys.Rev.Lett.* **102** (2009) 051101, [[arXiv:0810.4994](#)].
- [48] F. Halzen and D. Hooper, *The Indirect Search for Dark Matter with IceCube*, *New J.Phys.* **11** (2009) 105019, [[arXiv:0910.4513](#)].
- [49] **IceCube** Collaboration, R. Abbasi et al., *The design and performance of IceCube DeepCore*, *Astropart.Phys.* **35** (2012) [[arXiv:1109.6096](#)].
- [50] T. Sjöstrand, S. Mrenna, and P. Z. Skands, *A Brief Introduction to PYTHIA 8.1*, *Comput.Phys.Commun.* **178** (2008) 852–867, [[arXiv:0710.3820](#)].
- [51] N. Bell and K. Petraki, *Enhanced Neutrino Signals from Dark Matter Annihilation in the Sun via Metastable Mediators*, *JCAP* **04** (2011) 003, [[arXiv:1102.2958](#)].
- [52] A. Friedland, *On the Evolution of the Neutrino State Inside the Sun*, *Phys.Rev.* **D64** (2001) 013008, [[hep-ph/0010231](#)].
- [53] **Particle Data Group** Collaboration, K. Nakamura et al., *Review of Particle Physics*, *J.Phys.* **G37** (2010) 075021.
- [54] **T2K** Collaboration, K. Abe et al., *Indication of Electron Neutrino Appearance from an Accelerator-produced Off-axis Muon Neutrino Beam*, *Phys.Rev.Lett.* **107** (2011) 041801, [[arXiv:1106.2822](#)].
- [55] **Daya Bay** Collaboration, F. An et al., *Observation of electron-antineutrino disappearance at Daya Bay*, [[arXiv:1203.1669](#)].
- [56] L. Wolfenstein, *Neutrino Oscillations in Matter*, *Phys.Rev.* **D17** (1978) 2369–2374.
- [57] S. Mikheev and A. Smirnov, *Resonance enhancement of oscillations in matter and solar neutrino spectroscopy*, *Sov. J. Nucl. Phys.(Engl. Transl.)* **42** (1985).
- [58] S. Toshev, *Exact Analytical Solution of the Two Neutrino Evolution Equation in Matter with Exponentially Varying Density*, *Phys.Lett.* **B196** (1987) 170.
- [59] A. Strumia and F. Vissani, *Neutrino masses and mixings and...*, [[hep-ph/0606054](#)].
- [60] R. Lehnert and T. J. Weiler, *Neutrino Flavor Ratios as Diagnostic of Solar WIMP Annihilation*, *Phys.Rev.* **D77** (2008) 125004, [[arXiv:0708.1035](#)].
- [61] S. Mikheev and A. Smirnov, *Resonance oscillations of neutrinos in matter*, *Sov.Phys.Usp.* **30** (1987) 759.
- [62] M. Kachelriess and R. Tomas, *Nonadiabatic level crossing in resonant and nonresonant neutrino oscillations*, *Phys.Rev.* **D64** (2001), no. 7 073002.
- [63] R. Gandhi, C. Quigg, M. H. Reno, and I. Sarcevic, *Ultrahigh-Energy Neutrino Interactions*, *Astropart.Phys.* **5** (1996) 81–110, [[hep-ph/9512364](#)].
- [64] S. Dutta, M. Reno, I. Sarcevic, and D. Seckel, *Propagation of Muons and Taus at High Energies*, *Phys.Rev.* **D63** (2001) 094020, [[hep-ph/0012350](#)].
- [65] J. F. Beacom, N. F. Bell, D. Hooper, S. Pakvasa, and T. J. Weiler, *Measuring Flavor Ratios of High-Energy Astrophysical Neutrinos*, *Phys.Rev.* **D68** (2003) 093005, [[hep-ph/0307025](#)].

- [66] **IceCube** Collaboration, J. Ahrens et al., *Sensitivity of the IceCube Detector to Astrophysical Sources of High Energy Muon Neutrinos*, *Astropart.Phys.* **20** (2004) 507–532, [[astro-ph/0305196](#)].